pH-Dependent Conformations of the Amyloid β(1−28) Peptide Fragment Explored Using Molecular Dynamics†

Kent Kirshenbaum‡ and Valerie Daggett*

Department of Medicinal Chemistry, BG-20, University of Washington, Seattle, Washington 98195

Received August 24, 1994; Revised Manuscript Received March 6, 1995⊗

ABSTRACT: Molecular dynamics simulations were used to successfully reproduce the experimentally observed pH-dependent conformational behavior of a monomeric peptide in aqueous solution. Simulations were conducted at 298 K on a peptide corresponding to residues 1−28 of the amyloid β-peptide [referred to as β(1−28)], which is the primary component of the plaques associated with Alzheimer's disease. β(1−28) was found to be entirely α-helical at low pH. Upon deprotonation of acidic residues at medium pH, helical structure was lost in the N-terminal region. At high pH, some secondary structure was recovered to yield two helices joined by a kink. These results are in good agreement with the NMR solution structure at low pH [Zagorski and Barrow (1992) *Biochemistry 31,* 5621−5631; Talafous et al. (1994) *Biochemistry 33,* 7788−7796] and CD and NMR evidence of an α-helix to β-sheet transition at mid-range pH [Barrow et al. (1992) *J. Mol. Biol. 225,* 1075−1093]. Additional simulations were also able to regenerate folded species from partially unfolded conformers. A mechanism for the pH-dependent structural rearrangements is proposed that involves the creation of a hydrogen-bonded pair between Ser 8 and Glu 11. The evidence for the existence of a multiconformational equilibrium of folded and unfolded species of the peptide is discussed.

Alzheimer's disease (AD) is characterized by extracellular amyloid plaques, whose principle protein component is the amyloid β-peptide (39−42 residues; Glenner & Wong, 1984). The extent of accumulation of β-peptide in amyloid plaques correlates with the severity of dementia in Alzheimer's disease (Flood et al., 1991), which suggests that the β-peptide is directly involved in the pathogenesis of the disease. The β-peptide is a proteolytic product of the amyloid precursor protein, and different lengths are found depending on the processing. β(1−39), which contains the first 39 residues, is the major component of cerebrovascular deposits and other tissues (Joachim et al., 1989; Prelli et al., 1988), while β-(1−42) is the predominant form in plaques (Glenner & Wong, 1984; Masters et al., 1985; Kang et al., 1987).

Until recently, it was thought that the β-peptide was insoluble and a result of abnormal proteolysis, such that it would spontaneously self-assemble into β-sheets, the structure found in amyloid fibrils from AD brains (Kirschner et al., 1986). However, it has now been shown that the β-peptide is soluble (Halverson et al., 1990; Barrow & Zagorski, 1991; Barrow et al., 1992) and may be a normal proteolytic product that aggregates to form plaques as a result of abnormal changes in the microenvironment of the brain in patients with Alzheimer's disease [for example, by changes in the concentration of metal ions (Candy et al., 1986; Mantyh et al., 1993), temperature, pH (Yates et al., 1990), or other endogenous compounds such as proteoglycans (Snow et al., 1990; Fraser et al., 1992)]. Therefore, the hypothesis based on these observations is that local environmental changes may accelerate plaque formation and compete with normal proteolysis in aged and Alzheimer's disease patients.

It has been proposed that the N-terminal residues of the β-peptide, β(1−28), confer amyloidogenic potential in the solid state (Fraser et al., 1991a; Gorevic et al., 1987; Kirschner et al., 1987). Likewise, the hydrophobic C-terminal segment β(34−42) has been implicated (Halverson et al., 1990). Also, fibril assembly and disassembly is dependent on pH, occurring between pH 4 and pH 8 (Burdick et al., 1992; Fraser et al., 1991b). Interestingly, in an aqueous solution of a membrane mimicking solvent the β(1−28) peptide adopts partial α-helical structure (Hollosi et al., 1989; Barrow & Zagorski, 1991). Furthermore, Hilbich et al. (1991) found that the β(10−43) peptide forms a dimer that contains 80% β-sheet structure. Recently, it was demonstrated that the specific formation of β-structure correlates with neurotoxicity (Simmons et al., 1994).

In further studies of the conformational properties of the β-peptide, Zagorski and co-workers found that the N-terminal portion, β(1−28), of the peptide does not have a dominant conformation in solution and, instead, preferentially adopts random coil, α-helical, or β-structure depending on the temperature and solvent conditions [e.g., pH and trifluoroethanol (TFE) concentration] (Barrow et al., 1992). This region contains a mixture of polar and nonpolar residues and appears to mediate conformational transitions. The C-terminal region adopts β conformations exclusively and is thought to drive the aggregation of β-structure responsible for the plaques. But, detailed structural information for the fragments is limited to 2-D NMR studies of the β(1−28) peptide at low pH (Zagorski & Barrow, 1992). In fact, to quote Barrow et al. (1992) discussing their work, "The

† This work was supported by Alzheimer's Disease Research, a program of the American Health Assistance Foundation, Rockville, MD.

* To whom correspondence should be addressed [telephone, (206) 685-7420; Fax, (206) 685-3252; E-mail, daggett@fitz.mchem.washington.edu].

‡ Present address: Department of Pharmaceutical Chemistry, University of California, San Francisco, CA 94143.

⊗ Abstract published in *Advance ACS Abstracts,* April 15, 1995.

0006-2960/95/0434-7629$09.00/0

present study underscores the need for further research into the conformation, dynamics and mechanisms of amyloidosis of β-peptide in solution and, in particular, for more detailed studies on a molecular level." One approach to elucidate detailed dynamical and structural information for conformationally mobile species is through theoretical studies. We have undertaken molecular modeling studies to complement and extend the experimental solution studies of the β-peptides.

Molecular dynamics (MD) simulations have proved to be of utility in characterizing peptide structure and conformational properties in solution (Daggett et al., 1991a; DiCapua et al., 1991; Soman et al., 1991, 1993; Tirado-Rives & Jorgensen, 1991; Daggett & Levitt, 1992; De Loof et al., 1992; Brooks & Case, 1993; Hirst & Brooks, 1994). In the present study, we describe modeling of the pH-dependent conformations of the $\beta(1-28)$ peptide using such an approach. Simulations were conducted in water at 25 °C (298 K) at three pH ranges. Alteration of the ionization state of the appropriate side chains of $\beta(1-28)$ yields structures that display the conformational transitions observed by CD and NMR measurements, despite the simplicity of the treatment of pH. Molecular dynamics calculations provide a complete analysis of macromolecular motion at the atomic level; this has allowed a detailed mechanism for the pH-dependent conformational behavior to be proposed, which is, of course, subject to experimental verification. While the results of the simulations and the available experimental data are in good agreement, we must point out that due to limited conformational sampling accurate analysis of equilibrium properties is difficult. This means that we are often limited to investigating a subset of the conformers that may be present at equilibrium. Variation of the starting structures used to initiate the molecular dynamics simulations was conducted to better explore conformational space, and these efforts have provided information regarding the importance of folded, partially folded, and unfolded species.

METHODS

Molecular dynamics simulations were performed on the $\beta(1-28)$ peptide (sequence: DAEFRHDSGYEVHHQKLVFFAEDVGSNK) utilizing the program ENCAD (Levitt, 1990). The protocols (Daggett & Levitt, 1992) and potential function (Levitt, 1983, 1989; Levitt et al., 1995a,b) have been described. Molecular dynamics was conducted at 298 K. All solute and solvent atoms were treated explicitly. Water molecules were added around the peptide to fill a rectangular box with walls at least 8 Å from any peptide atom; this typically required the addition of approximately 2000 water molecules (the actual number depending on the starting structure and is given below) into a rectangular box about $30 \times 30 \times 60$ Å.

Solute and solvent systems were independently prepared for molecular dynamics. First, 2000 cycles of conjugate gradient energy minimization were performed on the water molecules alone. MD was then performed on the water molecules for 2000 steps, followed by an additional energy minimization of 2000 cycles. The peptide atoms alone were then energy minimized for 2000 cycles, followed by a minimization of the entire system for 2000 cycles. MD was initiated by bringing the entire system to equilibration at 298 K by scaling the velocities, which required 2−4 ps. After this procedure, classical MD was performed, and the energy of the system was conserved throughout the simulation. No further scaling of velocities was necessary. Periodic boundary conditions were used and the box volume was held constant. MD was performed with a time step of 2 fs, and atomic coordinates were saved every 100 steps (every 0.2 ps). An 8 Å nonbonded cutoff was employed, and the nonbonded list was updated every five steps. The simulation was allowed to continue until the overall secondary structure of the peptide was observed to be essentially stable over the course of 100 ps. In every case, the simulation was allowed to proceed for at least 500 ps.

Three types of starting structures were used:

(1) Initial investigation of the pH-dependent conformational behavior was performed using an all-helical starting structure, with (ϕ, ψ) angles of an ideal α-helix (-60°, −40°, respectively). Changes in pH were modeled by altering the ionization states of the relevant side chains (Asp, Glu, His) corresponding to a low, medium, and high pH range (pH 2−4, 5−6, and 8−9, respectively; see Table 1). These systems contained 1857 water molecules.

(2) Subsequent simulations sought to explore conformational space at low and high pH by initiating trajectories beginning from partially helical conformations. These structures were obtained by extracting peptide coordinates from three time points (25, 50, and 200 ps) along the medium pH simulation, which resulted in partial unfolding of the helix. These medium pH "aliquots" were adjusted to low and high pH by appropriate alterations of the side chains, subjected briefly to energy minimization, and then MD simulations were reinitiated at the new pH state. The systems contained the following numbers of water molecules: 1904 for the structure extracted at 25 ps, 2025 at 50 ps, and 1984 for the 200 ps starting structure.

(3) Further exploration of conformational space was accomplished by performing a simulation of the unfolded state at low and medium pH. The simulation was initiated from an idealized fully extended structure, with all (ϕ , ψ) angles at (180°, 180°). These simulations contained 3311 waters.

Trajectories were monitored primarily by analysis of the extent to which α-helical secondary structure was maintained or adopted by $\beta(1-28)$, using a method first described by Daggett et al. (1991b). A segment of the $\beta(1-28)$ peptide was defined to be helical when the (ϕ , ψ) angles of at least three consecutive residues were consistent with helical parameters ($-100° \leq \phi \leq -30°$, $-80° \leq \psi \leq -5°$) (Daggett et al., 1991b; Daggett & Levitt, 1992), and noncontiguous helical segments were allowed.

RESULTS AND DISCUSSION

Overall pH-Dependent Conformational Properties of the Peptide. In an effort to understand the pH-dependent conformational properties of the $\beta(1-28)$ amyloid peptide, simulations were performed at three different pH states. The starting structure in each case was an ideal α-helix. Changes in pH were modeled by adjustment of the ionization states of relevant side chains corresponding to low, medium, and high pH (Table 1). The simulations revealed that the conformational characteristics of this peptide were highly sensitive to pH conditions.

Table 1: Summary of Simulations Performed

pH	α-helix content of starting conformation[a] (%)	ionization state of residues	simulation time[b] (ps)
low	100	Asp^0, Glu^0, His^+	500
	88		(25+) 475
	65		(50+) 450
	69		(200+) 400
	0		500
medium	100	Asp^-, Glu^-, His^+	600
	0		500
high	100	Asp^-, Glu^-, His^0	500
	88		(25+) 475
	65		(50+) 450
	69		(200+) 300

[a] The starting conformations with less than 100% α-helix were extracted from the medium pH simulation and correspond to the following time points: 88% = 25 ps; 65% = 50 ps; and 69% = 200 ps (described further in the text). The starting structure with 0% α-helix was started in a fully extended conformation. [b] The time given in parentheses is when the snapshot was extracted from the medium pH simulation; the total simulation time for these systems begun from partially folded conformations is the sum of the two times listed.

Quantitative evaluation of the trajectories was based primarily on the extent to which the peptide retained its initial all α-helical structure. A plot of percent repeating helical content [i.e., three or more consecutive residues with α-helical (ϕ, ψ) values] as a function of simulation time is shown in Figure 1. At low pH the helical structure was well maintained throughout the simulation. From 400 to 500 ps of the low pH simulation, the β(1−28) peptide had an average of 99% repeating helical structure (Table 2). Deprotonation of the glutamate and aspartate side-chain carboxyl groups had a marked effect on the peptide's dynamic behavior. Under this "medium" pH condition, some helical structure was lost over the course of the first 100 ps, yielding a stable structure with a 68% helix content. High pH conditions yielded a helical content between the low and the medium pH states of 83%. The partial unfolding of the helix took place gradually over the first 200 ps. Figure 1 also shows that the high pH simulation was able to sample conformations of diminished helical content comparable to the medium pH state and return to more structured conformations.

While the time course of the helix content reflects the dynamics, stability, and unfolding behavior of the peptide, the distribution of helical structure along the sequence is also of interest (Figure 2). At low pH, all of the residues had (ϕ, ψ) angles consistent with α-helical parameters for more than 90% of the last 100 ps. At medium pH, helical structure was lost primarily in the N-terminal region from residues 1 to 8, and only the arginine of residue 5 of this segment yielded a significant amount of local helical structure. Residue 9 was at the junction between the unfolded and folded segments and was helical for ~40% of the time. All of the residues in the C-terminal two-thirds of the peptide were consistent with helical parameters throughout the simulation. At high pH, local helical structure was observed in the region from residues 3 to 7, while residues 8 and 9 were nonhelical. Residues 10−28 also displayed primarily helical parameters, with some transient "fraying" near the C-terminus.

A cartoon rendering of the final structures generated for each simulation illustrates that at low pH a helical structure was conserved throughout the length of the peptide (Figure 3). At medium pH, the N-terminal third of the peptide was unfolded, while the C-terminal portion retained a helical conformation. At high pH, two helical segments were joined by a kink a third of the way from the N-terminus of the peptide. The helical character of the C-terminal segment from residues 10 to 28 was evident at all pH conditions.

Variation of Initial Coordinates and Sampling of Conformational Space. Retention of helical structure in these simulations could either represent a realistic depiction of a native-like conformation or a locally favorable energetic minimum with a relatively high barrier to rupture of the α-helical hydrogen bond network. In order to more fully sample conformational space and to investigate the nature of the conformational transitions that drive helix unfolding, trajectories at low and high pH were also initiated from partially deformed conformations extracted from the medium pH run. The atomic coordinates for the β(1−28) peptide structure at 25, 50, and 200 ps into the medium pH run were extracted, the ionization states of the side chains were altered, and the simulations were resumed at the "new" pH conditions. The trajectories were continued for 300−475 ps to yield a total of 500 ps for each simulation (Table 1).

Regardless of the starting conformation, the total secondary structure content was stable over at least the last 100 ps of the simulation and generally for 400 ps (Figure 4). The 25 and 50 ps structures from the medium pH "unfolding pathway" refolded when placed under low pH conditions (Figure 4A). Re-formation of helical structure occurred rapidly, within 20 ps. This rearrangement consisted of acquisition of helical parameters in the "frayed" region of the peptide near the N-terminus at residues 2, 3, and 4. The 50 ps structure abstracted from the medium pH run was extensively unfolded throughout the N-terminal third of the peptide. However, molecular dynamics at low pH quickly (within a few picoseconds) reestablished helical parameters in all residues except 2 and 3. The simulations resulted in an intact helix after 50 ps of additional MD. A trajectory obtained by simulating the 200 ps medium pH structure at low pH was not able to "refold", and the 69% helical content of the medium pH simulation was maintained (Table 2). These results suggest that a conformational transition occurs between 50 and 200 ps along the medium pH trajectory that provides a barrier to re-formation of the α-helix (see below).

The dynamic behavior of the β(1−28) peptide at low pH was further investigated by performing a simulation starting with a fully extended chain. Initial minimization, prior to MD, generated a conformation that had no α-helical structure, but 16 residues were consistent with local β-structure. No repeating α-helical structure was established over the 500 ps time course of this simulation, and much of the local β-sheet content was rapidly lost within the first 75 ps (data not shown). After this point, the amount of β-sheet structure continued to decrease slowly. Over the last 100 ps, the β-content was 27%, including a four-residue segment from positions 10 to 13 that was intact more than 80% of the time.

The same 25, 50, and 200 ps medium pH structures were also used to probe conformational space at high pH (Figure 4B). The 25 ps structure began the simulation with 88% repeating helical structure, which rose to 95% averaged over the last 100 ps (Table 2). Interestingly, it took approximately 75 ps to re-form the helix at high pH but only 20 ps at low pH (compare panels A and B of Figure 4). The structures obtained at 50 and 200 ps into the medium pH run did not refold significantly at high pH and contained helical contents

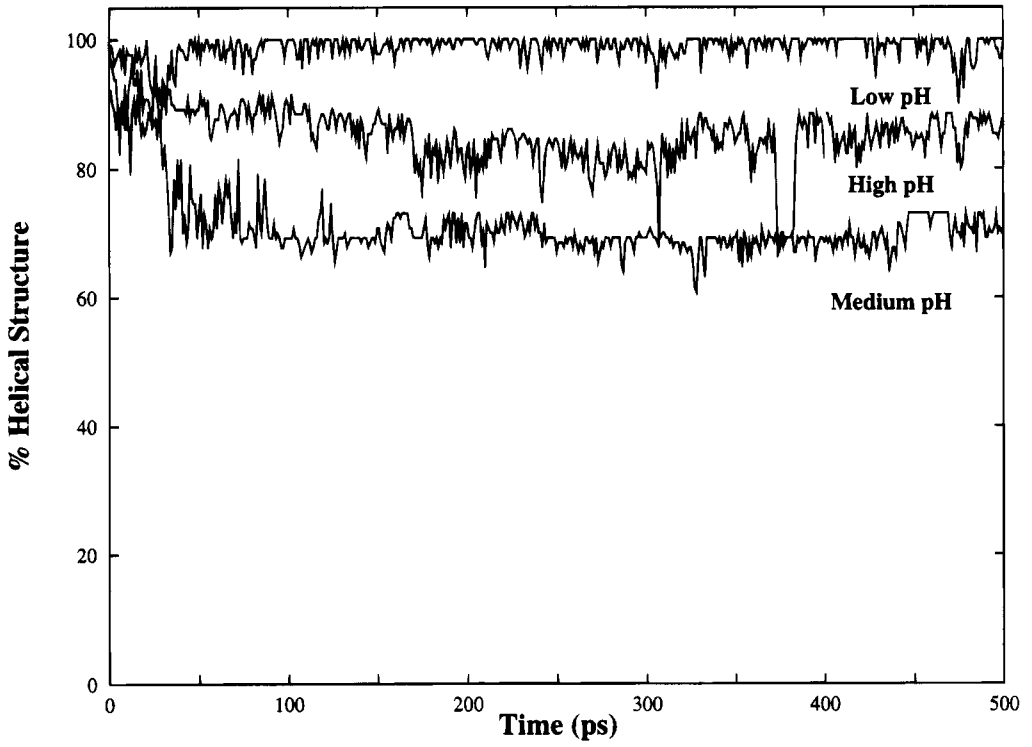

FIGURE 1: Percentage of repeating α-helical structure as a function of time and pH.

Table 2: α-Helix Content Determined from the Molecular Dynamics Simulations[a] and Using Circular Dichroism Spectroscopy

pH	α-helix content of starting conformation[b] (%)	⟨MD⟩[c] (%)	experiment[d] (%)
low pH	100	99	
	88	100	
	65	99	
	69	69	
	0	0	
	ensemble	66	56
medium pH	100	68	32
	0	0	
high pH	100	83	45
	88	95	
	65	71	
	69	71	

[a] Averages given for the final 100-ps portion of the simulations. [b] The starting conformations with less than 100% α-helix were extracted from the medium pH simulation (described further in the text). The starting structure with 0% α-helix was started in a fully extended conformation. [c] The average helical content over the last 100 ps of each simulation. [d] The helix content given is taken from Barrow et al. (1992).

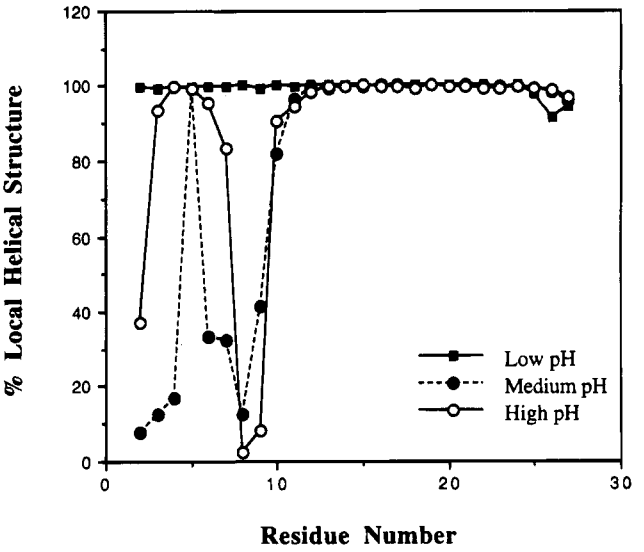

FIGURE 2: Percentage of local α-helical structure as a function of residue number at low, medium, and high pH.

of 71%. The distribution of local helical structure along the sequence for these simulations was virtually identical to that at medium pH (Figure 2).

In addition to the simulations at low and high pH beginning from alternate starting conformations, a simulation at medium pH starting from a 0% helix, extended chain was performed. The β-content was fairly high at 45%, relative to the comparable simulations at low pH (27%). Some β-structure was also adopted in the medium pH simulations starting with an ideal α-helix, ~10%, which was localized to the N-terminus. Thus, the medium pH conditions not only promote disruption of the α-helical structure but also support the formation of β-structure.

Specific Side-Chain Conformational Properties in the α-Helical State. The final structures from the MD trajectories demonstrate that the simulated global conformation of the β(1−28) peptide is dependent on the ionization state of the amino acid side chains (Figure 5). The unfolding of the helical structure at medium and high pH occurred in the highly charged N-terminal portion of the peptide. Assessment of the relative orientation of the charged groups provides insight into the forces that determine the pH-dependent conformational properties of this peptide.

The orientations of the side chains at low pH were constrained by the intrinsic geometry of the all-helical conformation. The $i \rightarrow i + 4$ spacing of side chains along the peptide created an unusual arrangement near the N-terminus. As can be seen in Figure 5, one face of the helix was comprised of the acidic side chains Glu 3, Asp 7, and Glu 11. Averaged over the last 100 ps of the simulation, the distance from C_δ of Glu 3 to C_γ of Asp 7 was 7.0 Å; the corresponding distance between Asp 7 and Glu 11 was 6.3

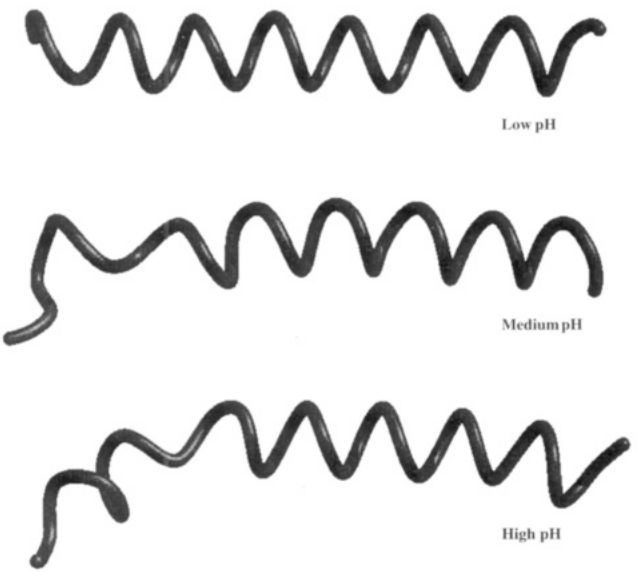

FIGURE 3: Ribbon representations of snapshots taken from the simulations at 500 ps. Computer graphics figures were generated using UCSF MidasPlus (Ferrin et al., 1988).

Å. Glu 22 resides on the same face of the helix as this trio of acidic residues. The basic Arg 5, His 6, His 13, and His 14 residues lie on the other side of the helix and constitute a highly positively charged face at low pH. A hydrophobic surface is located in the C-terminal portion of the peptide, comprised of residues Leu 17, Val 18, Phe 20, Ala 21, and Val 24.

The trio of acidic residues that comprised a compact structural element at low pH was located in the region of the $\beta(1-28)$ peptide that became unfolded at elevated pH. This would suggest that as these side chains become ionized, the repulsive interactions between the negatively charged carboxylates would drive the observed conformational rearrangements. Such was not the case. While Glu 3 and Asp 7 did move slightly farther apart (7.0 Å at low pH vs 7.9 Å at medium pH; $3C_\delta$ to $7C_\gamma$), this was accompanied by a decrease in the distance between Asp 7 and Glu 11 (from 6.3 to 5.6 Å; $7C_\gamma$ to $11C_\delta$). However, this region of the peptide was the location of substantial changes in side-chain orientations. The charged carboxylate group of Glu 11 formed a hydrogen bond with the hydroxyl side chain of Ser 8, which we will refer to as a "serine cap". This contact was intact throughout the course of the medium pH simulation (average distance during the final 100 ps: 2.45 Å from $8O_\gamma$ to the nearest $11O_\epsilon$). The prevalence and relative position of this hydrogen bond suggested that this interaction plays a major role in determining structural properties of the peptide from residues 1 to 10.

This "intimate" hydrogen bond was not the only unusual feature of the local conformation about Glu 11 at medium pH. Asp 7 was also oriented to bring its side-chain carboxylate into very close proximity with the corresponding group of Glu 11. The mean distance between the closest $7O_\gamma$ to the nearest $11O_\epsilon$ was 3.9 Å (over the final 100 ps). This seemingly unfavorable interaction was possible because of two water molecules "bridging" the carboxylate oxygens (Figure 6). This unusual structure has been observed in other simulations (Dang & Pettitt, 1987; Bader & Chandler, 1992; Dang et al., 1992; Perkyns & Pettitt, 1994; Valdeavella et al., 1994; Cannon et al., 1994) and serves to mitigate electrostatic repulsion.

Although the helical conformation of the main chain was disrupted by the increase in pH, the relative distances between the positive charge sites were not appreciably altered. The configuration of amino acid side chains in the C-terminal portion of $\beta(1-28)$ was essentially the same as at low pH, as would be expected from the retention of the helical structure in this region. The change from low to medium pH conditions introduced six negative charge sites into this 28-residue peptide. It is not surprising that this would disrupt a large portion of the secondary structure observed at low pH. It is remarkable, however, that apart from the unusual interactions around Glu 11 the relative configuration of the ionizable side chains was not changed substantially. This allowed attention to be focused on the Ser 8-Glu 11 "cap" in the analysis of the high pH simulation and in assessing the structural rearrangements that led to helix unfolding.

The structure obtained at the end of the high pH trajectory showed that the previously described "kink" corresponds to the same intimately hydrogen-bonded Ser 8−Glu 11 pair found in the medium pH simulation. The nature of this interaction was virtually unchanged upon going to higher pH. However, Asp 7 was no longer in proximity to this pair; the mean distance between the two closest carboxylate oxygens of residues 7 and 11 increased from 3.9 to 7.6 Å. This movement, in addition to the kink formed in this region, caused Glu 11 to reside on a different face of the helix as Glu 3 and Asp 7, mitigating the electrostatic repulsion between these negatively charged groups. In comparison to the all-helical conformation, secondary structure was lost at residues 2 and 3. This appeared to be caused by displacement of the N-terminus away from the rest of the helix and into the solvent. As seen at medium pH, the relative configuration of the side chains in the C-terminal portion of the peptide was largely unchanged.

Mechanism for pH-Dependent Conformational Transitions. The creation of a cap between residues 8 and 11 upon ionization of the side-chain carboxyl groups interrupted the helical structure at this point in the sequence. By rotation of the dihedrals around Gly 9, the high pH structure was able to accommodate this cap by inserting a kink into the peptide with a minimal disruption of the secondary structure (Figure 5). This transition occurred early in the simulation, 15−25 ps, as monitored by the fluctuations in $\psi 8$ and $\phi 9$. The net result was two helices, both stabilized at their N-termini by the presence of acidic residues, Glu 3 and Glu 11.

At medium pH, the influence of the Ser 8−Glu 11 cap evoked a more substantial reorientation of the main chain. The dihedrals $\psi 8$ and $\phi 9$ showed the same rapid transition to nonhelical parameters, although this process occurred somewhat later in the simulation. The novel feature early in the medium pH simulation was the gradual rotation of $\psi 6$ and $\phi 7$. This motion took place between 40 and 120 ps into the simulation, which was similar to the time frame in which the secondary structure of the N-terminus was lost (Figure 1). Residue 6 is a positively charged histidine residue, which suggests that the difference in conformational behavior at this site in comparison to the high pH simulation may be attributed to the interaction of the imidizolium group with the nascent helix, beginning around residue 10. The extension of the peptide main chain subsequently allowed the reorientation of the side chain of Asp 7 closer to the

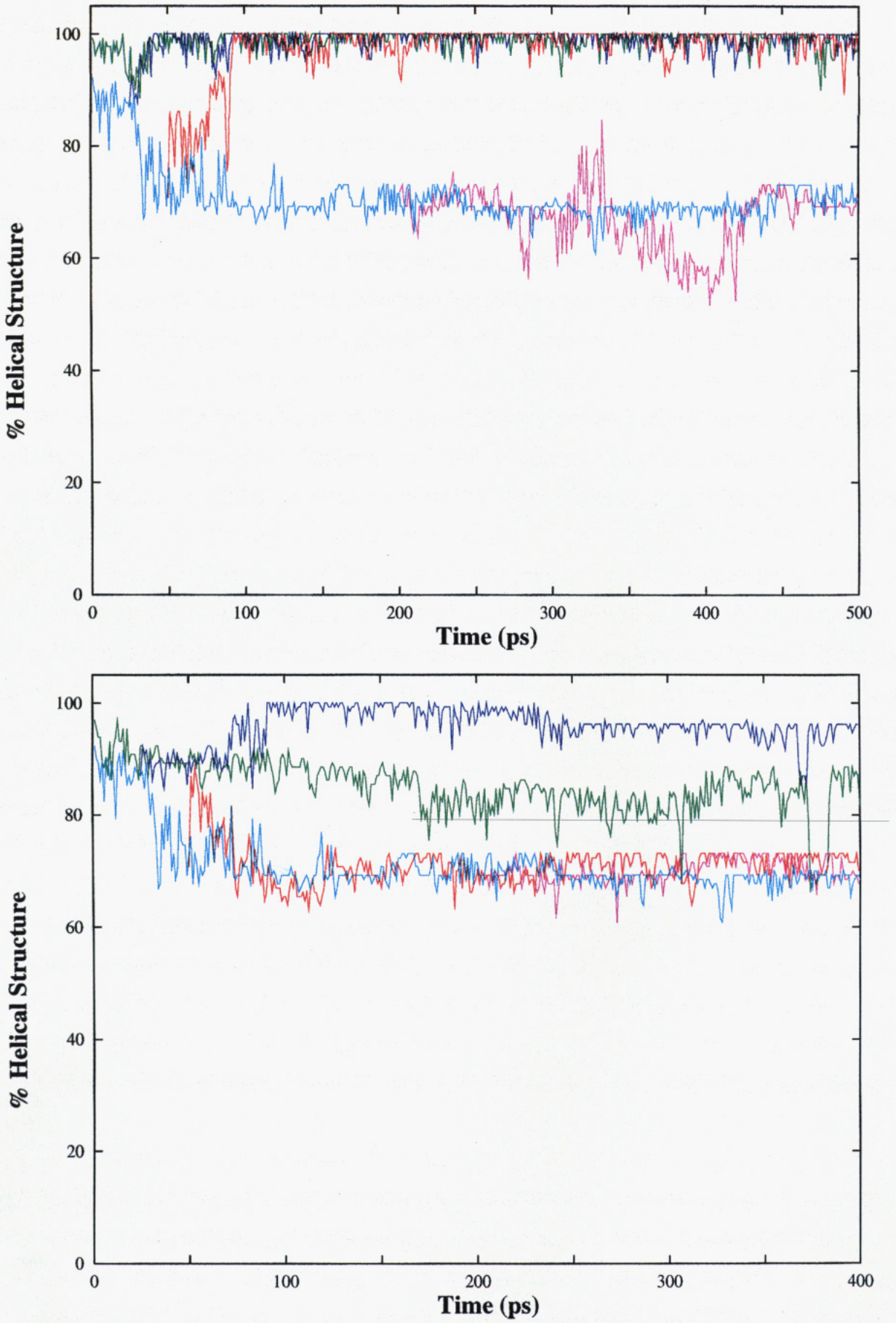

FIGURE 4: Percentage of repeating α-helical structure as a function of time at low pH (A, top) for different starting structures extracted from the medium pH run (100% helical starting structure in green, 85% α in blue, 65% α in red, 69% α in magenta) with the medium pH simulation shown for comparison (cyan). (B, bottom) Simulations at high pH initiated from structures extracted from the medium pH simulation, colored as described above.

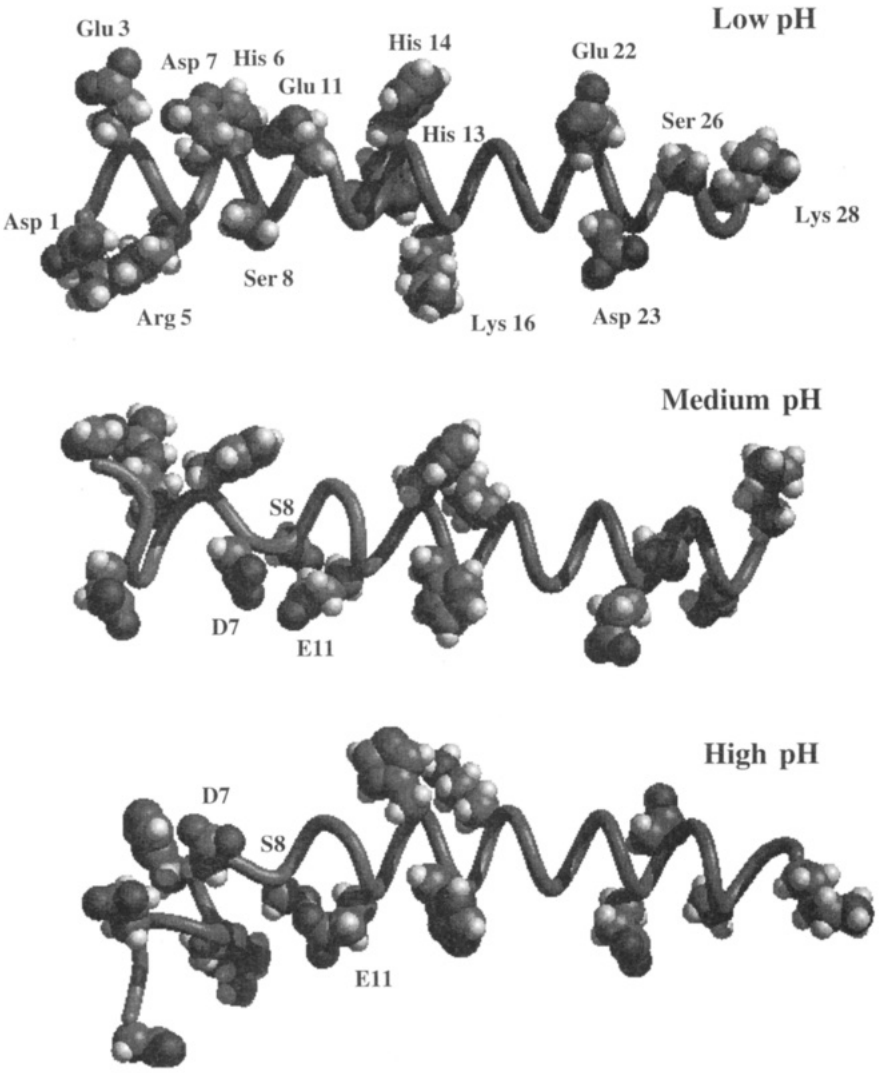

FIGURE 5: Snapshots taken at 500 ps with polar and charged residues displayed. In particular, attention is drawn to the serine cap interaction present at medium and high pH.

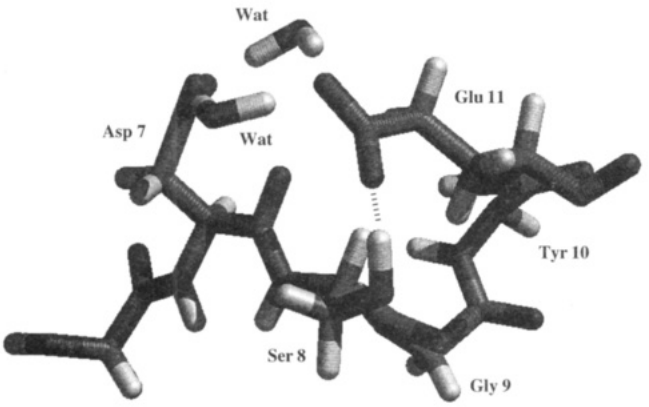

FIGURE 6: A closer view of the serine cap interaction depicted in Figure 5 showing the water molecules bridging the Asp 7 and Glu 11 carboxyl groups.

helix terminus to assume the unusual water-bridged structure with Glu 11 (Figure 6). This placed Asp 7 in the peptide axis and further disrupted the ability of the N-terminal residues to maintain their helical geometries. As $\beta(1-28)$ became further extended in this segment, water molecules were able to penetrate and form hydrogen bonds with the peptide backbone, resulting in loss of the remaining α-helical structure at the N-terminus.

The ability of structures extracted from 25 and 50 ps into the medium pH simulation to refold at low pH, and the inability of the 200 ps structure to do likewise, indicated that the dihedral rotations taking place after 50 ps were vital for maintaining nonhelical conformations. The above mechanism is discussed in more detail in the accompanying paper, which describes simulated mutations that substantiate the primacy of the Ser 8−Glu 11 cap in directing the pH-dependent conformational behavior.

Comparison to Experiment. Helical peptides are commonly found to exist as an ensemble of completely helical, disordered, and partially disordered states, which confounds spectral analysis of peptide structure (Merutka et al., 1993; see Discussion). Simulations were conducted on individual peptides under different conditions, not on populations. Because the time scale of the simulation was inadequate to observe transitions between folded and fully unfolded states, helical content measured for simulations initiated from a helical conformation would overpredict folded forms, and simulations initiated in an unfolded conformation would overpredict random structure.

The best comparison to experiment may be for that of an ensemble of the simulations initiated from helical, partially helical, and extended conformations. This is indeed found to be the case when considering experimental observables

reflecting the heterogeneity of the conformational ensemble (e.g., $^3J_{HN\alpha}$ coupling constants and CD) (Daggett & Kirshenbaum, 1995). For this reason, experimental properties discussed below are compared to a combination of the low pH simulations giving a 1:1 mixture of helical and nonhelical states [1 part each of the four helical simulations and 4 parts of the 0% helix, random coil simulation (Table 1); for example, the structures representing the last 100 ps of each simulation were pooled together, and properties were then evaluated for this new pool as if the structures were all sampled in a single simulation]. An optimal weighting of the simulations for comparison to the coupling constants yields an ensemble with a helix content of 66−73% (Daggett & Kirshenbaum, 1995).

In addition, we should note that the simulations were performed in water while many of the experimental studies were conducted in trifluoroethanol (TFE), a helix-stabilizing solvent. Recent experimental studies suggest that TFE shifts the conformational equilibrium of peptides to favor more structured, α-helical (Jasanoff & Fersht, 1994; Kippen et al., 1994) or β-states (Blanco et al., 1994). That is, TFE appears to bias the conformational ensemble in favor of structured states, but these states also exist but in lower concentrations in water. Thus, our 50% α-helical ensemble is similar to the TFE situation, and we could model the pure water situation by further diluting the ensemble with more nonhelical structures. Also, it should be noted that the helical content induced by TFE is saturated at approximately 30% in a variety of systems including the β-peptide, which corresponds to a mole fraction of 0.0995, or ~1 TFE molecule per 10 waters at 298 K. Therefore, simulations in water are reasonable alternatives to aqueous TFE solutions, although clearly not ideal. In addition, recent 2-D NMR studies of β(1−28) in non-TFE-containing solvent (dimethyl sulfoxide) confirm the results of Zagorski and co-workers (Sorimachi & Craik, 1994).

CD. CD spectra of the β(1−28) peptide in 60% trifluoroethanol (TFE) were collected at several pHs between 1.2 and 10.2 by Barrow et al. (1992). This study showed that the α -helical content was greatest at pH 1.2, with a value of 70%, and the value was 56% at pH 3.2, which is comparable to our low pH simulations (Table 2). Experimentally, the helical content dropped to a minimum of 32% at pH 5.4. Helical structure was then recovered as the pH was raised further, and at pH 8 it was 45%. Concurrent with loss of helix, β-sheet structure was adopted. No β-structure was observed at high or low pH conditions, but at pH 5.4 the peptide was estimated to have 60% β-sheet content.

The molecular dynamics simulations are in good qualitative agreement with the experimental results cited above, despite the fact that our simulations do not contain TFE molecules. The helix content was maximal at low pH, with an average of 99% of the residues demonstrating (ϕ, ψ) angles consistent with a helical conformation. Helical content then dropped to 68% at medium pH and was 83% at high pH (Table 2). Thus, while the overall trend in helical content as a function of pH is consistent with experiment, the amount of helical content was substantially larger than seen by CD in TFE. CD spectra report the signals generated from the entire pool of folded and unfolded species. The optimal combination of helical and nonhelical conformations at low pH, described above, results in a helix content of 66%, compared to an experimental value of 56%. Thus, consideration of an ensemble of structures yields reasonable agreement with experiment.

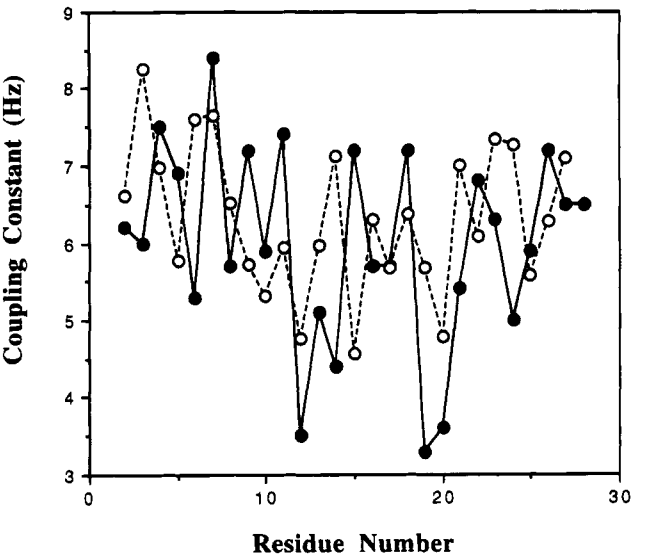

FIGURE 7: $^3J_{HN\alpha}$ coupling constants determined experimentally by Zagorski and Barrow (1992) and from a 50% helical ensemble of conformations at low pH (see text).

NMR. Zagorski and Barrow have obtained extensive information about the structural characteristics of the β(1−28) peptide at low pH using 2-D NMR (Zagorski & Barrow, 1992). Above pH 3, the β-peptide showed a tendency to aggregate. Determination of secondary structure at low pH was made on the basis of nuclear Overhauser enhancement (NOE) connectivities, resulting from the transfer of magnetization between protons close in space. In addition, vicinal coupling constants were determined.

Typically, the $^3J_{HN\alpha}$ coupling constants observed for α-helices are between 3.5 and 5.0 Hz (Wüthrich, 1986). Most of the $^3J_{HN\alpha}$ values reported for β(1−28) are between 5 and 7 Hz, and seven residues had values greater than 7 Hz. Such values are consistent with ϕ angles less than −80° (ie., verging on β-structure) and are generally regarded as being outside of stable α-helical geometries. Given that the NOE data (described below) are indicative of extensive α-helical structure, Zagorski and Barrow interpreted the large $^3J_{HN\alpha}$ values to be indicative of dynamic averaging between helical and extended chain conformations, especially in the N-terminal region of the peptide.

A comparison of vicinal coupling constants for each residue calculated from the simulation representing the 50% helical ensemble with the experimental values is shown in Figure 7. The coupling constants were calculated on the basis of the average ϕ values during the simulation using the Karplus relation ($^3J_{HN\alpha} = 6.4 \cos^2 \theta - 1.4 \cos \theta + 1.9$, where $\theta = |\phi - 60|$; Wüthrich, 1986). There is good agreement between experiment and the calculated coupling constants, and considering the inherent uncertainty in the two methods, the two curves in Figure 7 are indistinguishable. However, if only the α-helical conformations are considered, the calculated coupling constants are 4−5.5, which is substantially less than those determined experimentally. Thus, inclusion of nonhelical conformations is necessary to model these experimental data, and furthermore, the partially helical conformations generated in the simulation begun from the 200 ps medium pH structure were necessary to reproduce these data (data not presented). Therefore, the coupling

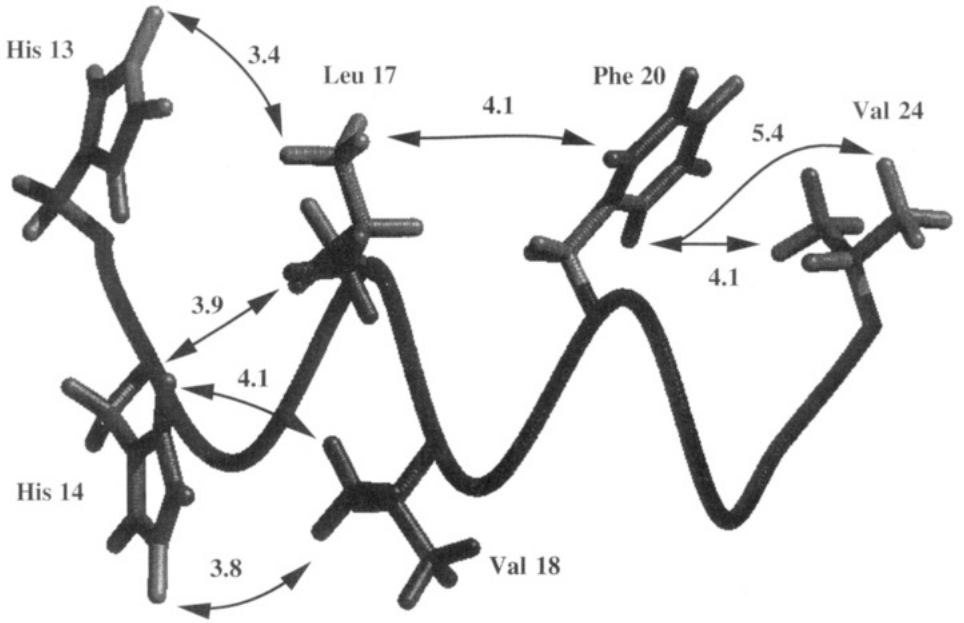

FIGURE 8: Medium-range side-chain NOE connectivities observed by Zagorski and Barrow (1992) at low pH with the appropriate proton−proton distances found for a 50% helical ensemble of conformations (see text).

constants are consistent with a population of structures composed of helical, partially helical, and nonhelical conformations—not just a mixture of 100% and 0% helical structures.

Extensive sequential and $i \rightarrow i + 3$ main-chain NOEs and medium-range $i \rightarrow i+4$ side-chain NOEs suggest that the $\beta(1-28)$ peptide exists in an entirely α-helical conformation (Figure 8) (Zagorski & Barrow, 1992). The absence of other long-range NOEs indicates that the peptide is linear and does not fold upon itself. Zagorski and Barrow (1992) interpreted these and other data to suggest that the all-helical conformation would be the predominant species at low pH, and as temperature or pH increased, a helix−kink−helix structure would be favored. They characterized this conformation as containing a solvent-exposed segment at Ser 8−Gly 9 that serves to connect the two α-helices. In addition, the disappearance of medium-range NOEs in the region 2−7 as the pH was increased to 3 indicated that as carboxylate groups become deprotonated, the conformational ensemble becomes heavily weighted with species that are unfolded throughout the N-terminal third of the peptide.

This description agrees with the results of the molecular dynamics simulations. The evidence for the presence of a mixture of folded and partially folded species is suggested by consideration of predicted coupling constants, as discussed above. However, molecular dynamics simulation conducted at low pH, albeit for a short period of time, showed that the starting structure is maintained under these conditions as an all-helical, linear peptide. Furthermore, at medium pH conditions, the simulation revealed that two substantial rearrangements of main-chain dihedrals in the N-terminal region allow the Ser 8−Gly 9 region to become solvent exposed and prompted unfolding of the helix in the region of residues 1−7. At high pH, which was not observable by 2-D NMR, the two-helix structure postulated by Barrow and Zagorski was observed in the molecular dynamics simulations. The two helices were joined by a kink at the location suggested by experiment, Ser 8−Gly 9.

The 2-D NMR spectrum obtained by Barrow and Zagorski at low pH revealed NOESY cross-peaks between protons located on the side chains of several residues. The corresponding distances from the simulation were obtained by weighted averaging ($\langle rw \rangle = \langle r^{-6} \rangle^{-1/6}$) over the last 100 ps for the 50% helical ensemble. These weighted distances were all in good agreement (≤5 Å) with experiment (Figure 8). Interestingly, all of these distances but one were greater than 10 Å for the nonhelical conformations, and the distances shown in Figure 8 are 20% higher, at most, than the values calculated from just the helical conformations (data not presented). Furthermore, all of the main-chain NOEs detected by Barrow and Zagorski were reproduced by the 50% helical ensemble (i.e., the appropriate proton−proton distances were ≤5 Å; data not presented).

These data substantiate the notion that the α-helical CD signal was diminished due to the presence of unfolded species. Furthermore, the discrepancy between the NOE signals, which suggested a fully helical peptide, and the $^3J_{HN\alpha}$ values, which indicate that there is a conformational ensemble, can be rationalized. NOE signals are proportional to the inverse sixth power of the distance between the interacting protons (Bax & Lerner, 1986) and are correspondingly heavily weighted toward those conformers with close contacts. That is, the NOEs "see" the folded conformers well and are relatively "blind" to the unfolded species. $^3J_{HN\alpha}$ values depend directly on the ϕ dihedral angle between interacting protons and will reflect the presence of unfolded structures to a greater degree.

These results demonstrate that molecular dynamics simulations were able to provide not only good qualitative agreement to experimentally determined overall secondary structure but also generated structures whose local conformations were in agreement with experimental parameters.

CONCLUSIONS

Due to the inherent limitations of computational processes, simulations have not, and cannot, assemble native folded conformations from primary sequence alone or from fully unfolded states. Accordingly, molecular dynamics of macromolecules generally begins from coordinates describing a

folded species. This presents a challenge for conducting molecular dynamics of peptides, which tend not to display the highly cooperative "all or none" structural behavior of larger proteins and thus seldom allow for the characterization of a single "native" conformation. The agreement between the results of the simulations of $\beta(1-28)$ conducted in the present study and experimental parameters obtained by Zagorski and co-workers indicate that this obstacle may be overcome.

At low pH, NOE connectivities suggest that the β-peptide has a high degree of α-helical structure. Agreement with experimental parameters that more fully reflect the peptide's multiconformational equilibria (CD and $^3J_{HN\alpha}$ coupling constants) was achieved by considering a conformational ensemble generated by simulations initiated from partially and completely folded states. Some of these simulations were able to refold to all-helical conformations, while other simulations provided information on the nature of the less-ordered species.

The influence of pH conditions on the results of molecular dynamics simulation is a topic that has not been given extensive treatment. The agreement with NMR data at low pH invites confidence that simulations conducted at medium and high pH are also reasonable representations of the structure of $\beta(1-28)$ at these conditions. The unfolding of the helix in the N-terminal region of the peptide at medium pH and the partial refolding of this region to yield a helix−kink−helix structure at high pH are in agreement with the limited experimental data. Thus, if the overall secondary structure of the peptide can be characterized under certain conditions (favorable pH, presence of structure-inducing solvent), this can be used as a starting point for simulations under conditions that generate partially unfolded conformations. In addition, the multiconformational equilibria between folded and unfolded conformers may be approximated by the appropriate averaging of simulations initiated from partially folded structures and completely extended structures.

An additional benefit of molecular dynamics simulations is the detailed structural information that can be obtained. This has allowed us to propose a mechanism for the pH-dependent structural transitions observed for $\beta(1-28)$, involving the creation of an intimately hydrogen-bonded pair between Ser 8 and Glu 11 at medium and high pH. Electrostatic repulsion around this pair causes helix dissociation in the N-terminal region at medium pH; deprotonation of histidine residues at high pH partially alleviates this unfavorable interaction, and some secondary structure is recovered. This mechanism has been tested by simulations of the pH-dependent structural behavior of $\beta(1-28)$ peptides with "mutations" at positions 8, 9, and 11 [see Kirshenbaum and Daggett (1995)].

The data presented here demonstrate that molecular dynamics simulations can reproduce the pH-dependent conformational behavior of the $\beta(1-28)$ peptide by merely adjusting the ionization state of the relevant amino acid side chains. The elucidation of the mechanism of these structural transitions may lead to understanding of the nature of the conversion of the full β-amyloid peptide from a soluble helical form to an insoluble β-sheet form in vivo. This behavior has been proposed to be pivotal in the process by which circulating β-peptide aggregates and deposits as amyloid plaque in the brains of individuals with Alzheimer's disease. The finding that the AD brain is significantly more acidic than found in control specimens (pH 6.6 vs 7.2; Yates et al., 1990) suggests that the cerebral microenvironment could play a role in "seeding" plaque formation. Simulations of multimeric complexes may provide further information on the molecular pathogenesis of this process at a structural level.

ACKNOWLEDGMENT

We thank Michael Zagorski for many helpful discussions, for providing data prior to publication, and for comments on the manuscript. Some of this work was performed at Reed College as part of an undergraduate thesis (K.K.), and we gratefully acknowledge the faculty of the Chemistry Department, especially Tom Dunne, Alan Shusterman, and Arthur Glasfeld, for making this possible and for valuable suggestions.

REFERENCES

Bader, J. S., & Chandler, D. (1992) *J. Phys. Chem. 96*, 6423−6427.

Barrow, C. J., & Zagorski, M. G. (1991) *Science 253*, 179−182.

Barrow, C. J., Yasuda, A., Kenny, P. T. M., & Zagorski, M. G. (1992) *J. Mol. Biol. 225*, 1075−1093.

Bax, A., & Lerner, L. (1986) *Science 232*, 960−967.

Blanco, F. J., Jimenez, M. A., Pineda, A., Rico, M., Santoro, J., & Nieto, J. L. (1994) *Biochemistry 33*, 6004−6014.

Brooks, C. L., & Case, D. (1993) *Chem. Rev. 93*, 2487−2502.

Burdick, D., Soreghan, B., Kwon, M., Kosmoski, J., Knauer, M., Henschen, A., Yates, J., Cotman, C., & Glabe, C. (1992) *J. Biol. Chem. 267*, 546−554.

Candy, J. M., Klinowski, J., Perry, R. H., Perry, E. K., Fairbairn, A., Oakley, A. E., Carpenter, T. A., Atack, J. R., Blesses, G., & Edwardson, J. A. (1986) *Lancet i*, 354−356.

Cannon, W. R., Pettit, B. M., & Cammon, J. A. (1994) *J. Phys. Chem. 98*, 6225−6230.

Chandler, D., & Andersen, H. C. (1972) *J. Chem. Phys. 57*, 1930.

Daggett, V., & Levitt, M. (1992) *J. Mol. Biol. 223*, 1121−1138.

Daggett, V., & Kirshenbaum, K. (1995) *Biopolymers* (submitted for publication).

Daggett, V., Kollman, P. A., & Kuntz, I. D. (1991a) *Biopolymers 31*, 285−304.

Daggett, V., Kollman, P. A., & Kuntz, I. D. (1991b) *Biopolymers 31*, 1115−1134.

Dang, L. X., & Pettitt, B. M. (1987) *J. Chem. Phys. 96*, 4046−4049.

Dang, L. X., Pettitt, B. M., & Rossky, P. J. (1992) *J. Chem. Phys. 96*, 4046−4047.

De Loof, H., Nilsson, L., & Rigler, R. (1992) *J. Am. Chem. Soc. 114*, 4028−4035.

DiCapua, F. M., Swaninathan, S., & Beveridge, D. L. (1990) *J. Am. Chem. Soc. 112*, 6768−6771.

Ferrin, T. E., Huang, C. C., Jarris, L. E., & Langridge, R. (1988) *J. Mol. Graphics 6*, 13−27.

Flood, J. F., Morley, J. E., & Roberts, E. (1991) *Proc. Natl. Acad. Sci. U.S.A. 88*, 3363−3366.

Fraser, P. E., Duffy, L. K., O'Malley, M. B., Nguyen, J. T., Inouye, H., & Kirschner, D. A. (1991a) *J. Neurosci. Res. 28*, 474−485.

Fraser, P. E., Nguyen, J. T., Surewicz, W. K., & Kirschner, D. A. (1991b) *Biophys. J. 60*, 1190−1201.

Fraser, P. E., Nguyen, J. T., Chin, D. T., & Kirschner, D. A. (1992) *J. Neurochem. 59*, 1531−1540.

Glenner, G. G. (1988) *Cell 52*, 307.

Glenner, G. G., & Wong, C. W. (1984) *Biochem. Biophys. Res. Commun. 120*, 885−890.

Goate, A., Chartler-Harlin, M. C., Mullan, M., Brown, J., Crawford, F., Fidani, L., Giuffra, L., Haynest, A., Irving, N., James, L., Mant, R., Newton, P., Rooke, K., Roques, P., Talbot, C., Williamson, R., Rossor, M., Owen, M., & Hardy, J. (1991) *Nature 349*, 704−707.

Golde, T. E., Estus, S., Younkin, L. H., Selkoe, D. J., & Younkin, S. G. (1992) *Science 255*, 728−730.
Goldgaber, D., Lerman, M. I., McBride, O. W., Saffiotti, U., & Gajdusek, D. C. (1987) *Science 235*, 880.
Gorevic, P. D., Castano, E. M., Sarma, R., & Frangione, B. (1987) *Biochem. Biophys. Res. Commun. 147*, 854−862.
Halverson, K., Fraser, P. E., Kirschner, D. A., & Lansbury, P. T., Jr. (1990) *Biochemistry 29*, 2639−2644.
Hilbich, C., Kisters-Woike, B., Reed, J., Masters, C. L., & Beyreuther (1991) *J. Mol. Biol. 218*, 149−163.
Hirst, J. D., & Brooks, C. L. (1994) *J. Mol. Biol. 243*, 173−178.
Hollosi, M., Otvos, L., Kajtar, J., Percell, A., & Lee, V. M.-Y. (1989) *Pept. Res. 2*, 109−113.
Jasanoff, A., & Fersht, A. R. (1994) *Biochemistry 33*, 2129−2135.
Joachim, C. L., Mori, H., & Selkoe, D. J. (1989) *Nature 341*, 226−230.
Johnson, W. C. (1990) *Proteins 7*, 205.
Kang, J., Lemaire, H. G., Unterbeck, A., Salbaum, J. M., Masters, C. L., Grzeschik, K. H., Multhaup, G., Beyreuther, K., & Muller-Hill, B. (1987) *Nature 325*, 733−736.
Kippen, A. D., Arcus, V. L., & Fersht, A. R. (1994) *Biochemstry 33*, 10013−10021.
Kirschner, D. A., Abraham, C., & Selkoe, D. J. (1986) *Proc. Natl. Acad. Sci. U.S.A. 83*, 503−507.
Kirschner, D. A., Inouye, H., Duffy, L. K., Sinclair, A., Lind, M., & Selkoe, D. J. (1987) *Proc. Natl. Acad. Sci. U.S.A. 84*, 6953−6957.
Kirshenbaum, K., & Daggett, V. (1995) *Biochemistry 34*, 7640−7647.
Levitt, M. (1983) *J. Mol. Biol. 168*, 595−620.
Levitt, M. (1989) *Chem. Scr. 29A*, 197−203.
Levitt, M. (1990) *ENCAD—Energy Calculation & Dynamics*, Stanford University and Yeda, Rehovot, Israel.
Levitt, M., Hirshberg, M., Sharon, R., & Daggett, V. (1995a) *Comput. Phys. Commun.* (in press).
Levitt, M., Hirshberg, M., Sharon, R., & Daggett, V. (1995b) *J. Am. Chem. Soc.* (submitted for publication).
Mantyh, P., Ghilardi, J., Rogers, S., DeMaster, E., Allen, C., Stimson, E., & Maggio, J. (1993) *J. Neurochem. 61*, 1171−1174.
Masters, C. L., Simms, G., Weinman, N. A., Multhaup, G., McDonald, B. L., & Beyreuther, K. (1985) *Proc. Natl. Acad. Sci. U.S.A. 82*, 4245−4249.
Merutka, G., Morikis, D., Brüschweiler, R., & Wright, P. E. (1993) *Biochemistry 32*, 13089−13097.
Nelson, J. W., & Kallenbach, N. R. (1986) *Proteins 1*, 211−217.
Palmer, A. G., & Case, D. A. (1992) *J. Am. Chem. Soc. 114*, 9059−9067.
Perkyns, J., & Pettitt, B. M. (1994) *J. Phys. Chem. 98*, 5147−5151.
Prelli, F., Castano, E. M., van Duinen, S. G., Bots, G. T. A. M., Luyendijk, W., & Frangione, B. (1988) *Biochem. Biophys. Res. Commun. 151*, 1150−1155.
Simmons, L. K., May, P. C., Tomaselli, K. J., Rydel, R. E., Fuson, K. S., Brigham, E. F., Wright, S., Lieberburg, I., Becker, G. W., Brems, D. N., & Li, W. Y. (1994) *Mol. Pharmacol. 45*, 373−379.
Soman, K. V., Karimi, A., & Case, D. A. (1991) *Biopolymers 31*, 1351−1361.
Soman, K. V., Karimi, A., & Case, D. A. (1993) *Biopolymers 33*, 1567−1580.
Sorimachi, K., & Craik, D. J. (1994) *Eur. J. Biochem. 219*, 237−251.
Snow, A. D., Mar, H., Nochlin, D., Sekiguchi, R. T., Kimata, K., Koike, Y., & Wight, T. N. (1990) *Am. J. Pathol. 137*, 1253−1270.
Talafous, J., Marcinowski, K. J., Klopman, G., & Zagorski, M. G. (1994) *Biochemistry 33*, 7788−7796.
Tirado-Rives, J., & Jorgensen, W. L. (1991) *Biochemistry 30*, 3864−3871.
Valdeavella, C. V., Perkyns, J. S., & Pettitt, B. M. (1994) *J. Chem. Phys. 101*, 5093−5109.
Wüthrich, K. (1986) *NMR of Proteins and Nucleic Acids*, Wiley, New York.
Yates, C. M., Butterworth, J., Tennant, M. C., & Gordon, A. (1990) *J. Neurochem. 55*, 1624−1630.
Zagorski, M. G., & Barrow, C. J. (1992) *Biochemistry 31*, 5621−5631.

BI941976P